High Efficiency and High-Power Quality Modulation Strategy for Single-Stage Electrolytic Capacitor-less On-board EV Charger

Million Gerado Geda, Tat-Thang LE, Sunju Kim, Kihoon Kim, Huu-Phuc Kieu, and Sewan Choi, Fellow, IEEE
Dept. Electrical & Information Engineering
Seoul National University of Science and Technology, Seoul 139-743 South Korea.
milliongerado1023@seoultech.ac.kr, schoi@seoultech.ac.kr

***Abstract* -- This article presents a modulation scheme for achieving high-efficiency and high-power quality based on the secondary duty cycle and the phase shift for a single-stage electrolytic capacitor-less bidirectional onboard charger. Zero voltage switching is achieved for all switches for wide voltage range operation based on an optimized duty cycle which increased the efficiency of the converter. Meanwhile, high power quality is guaranteed by a varying phase shift which is directly generated by a controller. To validate the proposed modulation scheme, experimental results from the 3.7kW onboard charger are provided at 1kW power showing an improvement of 0.4% over the conventional method. Furthermore, the efficiency of the converter is improved by 3% at low battery voltage where zero voltage switching is severe while using the conventional method.**

***Index Terms* -- Onboard charger, modulation scheme, zero voltage switching, high-efficiency, and high-power quality.**

I. INTRODUCTION

Nowadays, the demand for charging infrastructure is increasing with the global promotion of electric vehicles (EVs) as the solution to greenhouse gas emissions and fossil-fuel consumption. Single-stage bidirectional converters are a recent research topic since power factor correction (*PFC*) and dc-dc converter circuits are integrated to achieve low components count, low production cost, high power density, and high efficiency [1]-[5]. Therefore, single-stage converters are suitable for the application of EV chargers, UPS, ESS, etc.

Among single-stage converters, interleaved totem-pole structure [1] shown in Fig. 1 has high switches utilization factor, high power density, and a prominent future of achieving ripple-free grid current compared to other single-stage structures such as matrix-based [3] and indirect matrix-based [4] and [5] converters while using low input filter size when primary duty fixed 0.5.

Switch turn-on loss is a dominant switching loss in Silicon Carbide (*SiC*) [2]. That means that Zero Voltage Switching (*ZVS*) should be achieved for all switches to reduce switch turn-on-related power loss. In addition, ZVS is also good to minimize Electromagnetic Interference (*EMI*). Furthermore, high power quality, good dynamic tolerance, and control simplicity are recent research topics of single-stage converters.

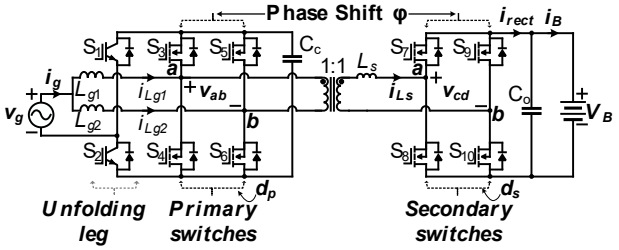

Fig. 1. Circuit of the single-stage *DAB* ac-dc converter [1].

Many efforts have been made to improve the performance efficiency of single-stage converters by using different modulation schemes and optimizations. Control optimization can be applied to available single-stage control variables which include phase shift between the primary and secondary side carrier (φ), primary duty (d_p), secondary duty (d_s), and switching frequency (f_{sw}).

In [4], a combined φ and f_{sw} modulation scheme was proposed, where two control variables; φ and d_s are obtained from the lookup table. The power is controlled by f_{sw}, which varies from 35 to 100kHz.

In similar ways, a modulation scheme involving four control variables was introduced in [5]. The power transfer is controlled by f_{sw} of a wide range variation from 150 to 500kHz. Besides, this control method is difficult to implement because three control variables φ, d_s, and d_p are obtained from the Lookup table of heavy calculations that require a large memory space.

A mode-by-mode control of φ and f_{sw} was introduced in [6] in which f_{sw} is varied from 70 to 100kHz, d_p is fixed at 0.5, and d_s is limited to rectified grid voltage shape. As a result, a narrow *ZVS* voltage range is achieved.

Similarly, an optimal reactive power control method was introduced [7] in which d_s is generated by the controller. Meanwhile, φ and f_{sw} are calculated based on d_s simultaneously. This method is good for reducing circulating current but not optimal for *ZVS* turn-on.

In [8], a single-loop control method of minimum current stress, and a soft switching method was introduced, but

none of the control variables is generated by the controller. Instead, φ, d_s, and d_p are obtained from calculations involving L_s that change with temperature which makes this method unrealistic.

A wide range f_{sw} variation is not good for the optimal designed operation of passive components. Besides, using a lookup table for more than one control variable is not good because a Lookup table is the result of a particular solution based on trial and error which uncovers the control system for external disturbance [9].

A simple modulation scheme involving a single control variable of dc φ which is directly output by the controller was introduced in [1]. The PFC was realized by a rectified grid voltage shape d_s. However, the resulting input grid current contains 3rd, 5th, 7th, etc. harmonic components which increased the *THD* of the grid current by over 10%, and a narrow ZVS turn-on was achieved.

In [2], a fourth-order harmonic was injected into d_s introduced in [1]. As a result, grid current THD was improved, but the *ZVS* turn-on of secondary switches become worse, particularly at low battery voltage.

This article presented a new modulation strategy for single stage ac-dc DAB converter by combining two optimal operations of control variables d_s and φ to:-

- Achieve full *ZVS* turn-on for all switches over a wide voltage range while achieving optimal transformer current to reduce conduction loss while using fixed f_{sw}.
- Achieve high power quality (low grid current THD).
- To reduce current stress and conduction loss.

II. Proposed Modulation Scheme, ZVS Range, and Power Analysis

Fig. 2 shows the key waveforms of the proposed modulation scheme. Primary duty d_p is fixed at 0.5 for achieving a ripple-free grid current. This means that switching frequency components in the grid current are suppressed due to the 180° interleaving operation of switches on primary side legs. The voltage across the clamp capacitor (v_{Cc}) is two times the rectified grid voltage as d_p is fixed at 0.5. The primary switching frequency voltage (v_{ab}) is constructed from v_{Cc} and the switching function of S_3 to S_6.

Similarly, the secondary side switching frequency voltage (v_{cd}) is constructed from V_B and the switching function of $S_7 \sim S_{10}$. The value of d_s is generated by a simple Lookup table to achieve a wide voltage range *ZVS* turn-on for all switches. Meanwhile, *PFC* is guaranteed by φ which is output by the controller. The peak value of φ determines the amount of power transfer. Meanwhile, the instantaneous shape of φ satisfies the power quality of the grid input current.

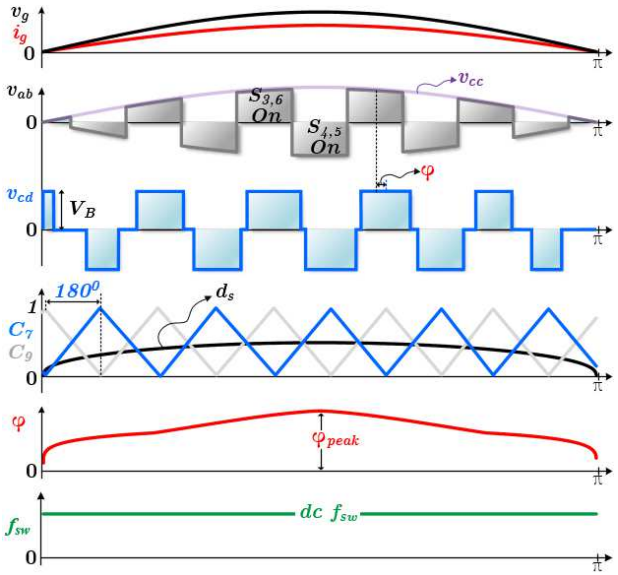

Fig. 2. The key waveforms showing how to construct v_{ab}, v_{cd}, and PFC realization.

A. ZVS conditions

The *ZVS* of the single-stage converter is highly determined by voltage gain (*M*), given in (1). This means that if *M*<<1, the primary switches can easily achieve *ZVS* turn-on, but secondary side switches operate with hard switching (*HS*) turn-on. Contrarily, if *M* >>1, the secondary switches can easily achieve *ZVS* turn-on, meanwhile primary switches operate with HS turn-on. However, when *M* is near unity, *ZVS* turn-on can be achieved for all switches.

In this article, *M* is adjusted near unity by changing d_s based on the lookup table, based on (1) and (2).

$$M = k\,\frac{volt\text{-}secof\ v_{ab}}{volt\text{-}sec\ of\ v_{cd}} = k\,\frac{d_s \cdot V_B}{d_p \cdot v_{Cc}} \tag{1}$$

$$k = f(n, L_s, f_{sw}, v_g, V_B) \tag{2}$$

Fig. 3 shows the *ZVS* turn-on currents of primary and secondary switches. Negative currents show that the switch current is negative during the switch turn-on. That means that the *ZVS* turn-on is achieved. Therefore, with the proposed method full *ZVS* turn-on is achieved for all

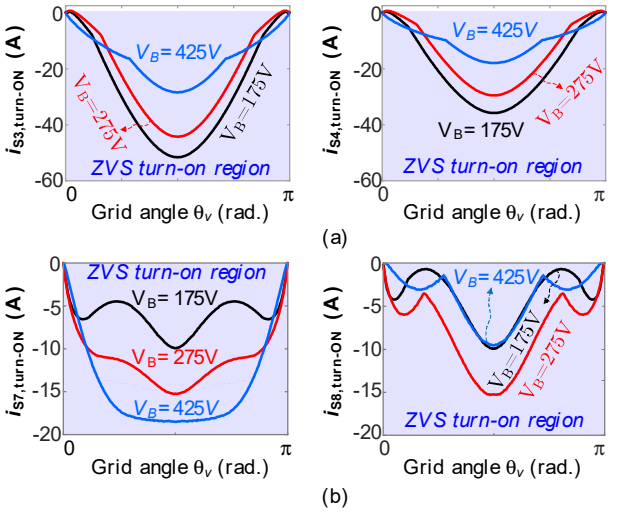

Fig. 3. ZVS turn-on current of (a) primary switches and (b) secondary switches.

switches from 175 to 425V battery voltage for an input grid voltage of 120V. That is also true for 350 to 850V battery voltage and 240V grid input voltage while scaling up input and output voltage by two times. That means that the scaling of input and output voltage does not change the *ZVS* turn-on operation of the converter.

B. Power analysis

In this section, the relationship between power and its control variables is presented mode by mode based on generalized *DAB* modeling, shown in Fig. 4 (a). Fig. 4 (b) shows an inner mode operation where the entire non-zero of v_{cd} is subscribed inside the non-zero of v_{ab} and vice versa. Fig. 4 (c) shows outer mode operation, where the non-zero of v_{ab} is partially outside of the non-zero of v_{cd}. The dual-phase shift (*DPS*) power analysis of the proposed converter was given in [1] only for outer mode operation by ignoring an inner mode operation. Therefore, the analysis of φ was not accurately provided to achieve optimal performance of the converter.

The value of the series inductor current $i_{Ls}(t)$ can be determined by substituting t_1 to t_4, illustrated in Fig. 4 (b) and Fig. 4 (c) in (3) at each point.

$$i_{Ls}(t_i) = \frac{v_{ab}(t)+v_{cd}(t)}{L_s}(t-t_i)+i_{Ls}(t_i) \tag{3}$$

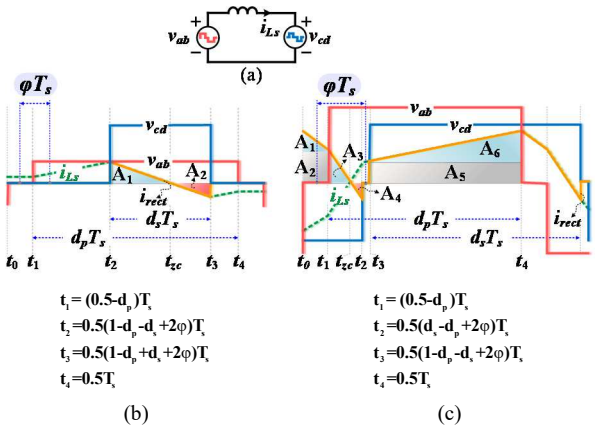

Fig. 4. (a) Electrical modeling of DAB. Switching frequency operation waveforms showing (a) Inner mode operation. (b) Outer mode operation.

An average value of i_{rect} can be determined as given in (4) and (5) for inner mode and outer mode, respectively. The area (A_i) inscribed under rectified i_{rect} is determined segment by segment considering the polarity of the i_{rect} into account. The negative i_{rect} shows backflow current, meanwhile, the positive i_{rect} shows charging current.

$$I_{rect[inner\ mode]} = \frac{2}{T_s}(A_1+A_2) \tag{4}$$

$$I_{rect[outer\ mode]} = \frac{2}{T_s}(A_1+A_2+A_3+A_4+A_5) \tag{5}$$

Finally, the power equations of inner mode and outer mode operations are given in TABLE I. The boundary phase shift (φ_b) of inner mode and outer mode operation is determined as given in (6).

TABLE I

POWER AND PHASE SHIFT EQUATION FOR INNER MODE AND OUTER MODE OPERATION

Modes	Inner mode	Outer mode
Conditions	$\varphi<\varphi_b$	$\varphi>\varphi_b$
Power	$\frac{2V_B\lvert v_g\rvert d_s\varphi}{L_s f_s(1-d_p)}$	$\frac{V_B\lvert v_g\rvert\left[8\varphi^2-4\varphi-2d_p^2+2d_p-2d_s^2+2d_s+1\right]}{4L_s f_s(1-d_p)}$
φ	$\frac{L_s f_s\lvert i_g^*\rvert(1-d_p)}{2V_B d_s}$	$\frac{1}{4}-\frac{1}{2}\sqrt{\frac{1}{4}-d_p^2+d_p-d_s^2+d_s-\frac{2L_s f_s\lvert i_g^*\rvert(1-d_p)}{nV_B}}$

$$\varphi_b = (0.5-\theta-d_s)\pi \tag{6}$$

The power analysis provided in this section does not consider the effect of dead time, power loss, and other parasitic parameters for simplicity. Furthermore, due to the dependency of calculated φ on L_s, it is difficult to directly use for power regulation. Therefore, this article introduced real-time power regulation by using controllers.

III. CONTROL BLOCK DIAGRAM

Fig. 5 shows the proposed control block diagram consisting of two control loops which are the outer loop and inner loop controller. The outer loop generates the command grid peak current (I_g^*) in constant current (*CC*), constant power (*CP*), and constant voltage (*CV*) charging mode. In *CC* operation modes I_g^* is determined by a limiter. However, in *CP* and *CV* modes, I_g^* is below limited value, so output by the controller. *PLL* is used to generate normalized ac command current which is multiplied by I_g^* to generate ac command current (i_g^*) for unity *PF*. Switching frequency and noise signals are used to be filtered out from sensed grid current to avoid unwanted signals before input to the controller.

In [1], the grid input current consists of odd-order harmonics (3rd, 5th, 7th, etc.) because the non-linear relationship between power and its control variables is

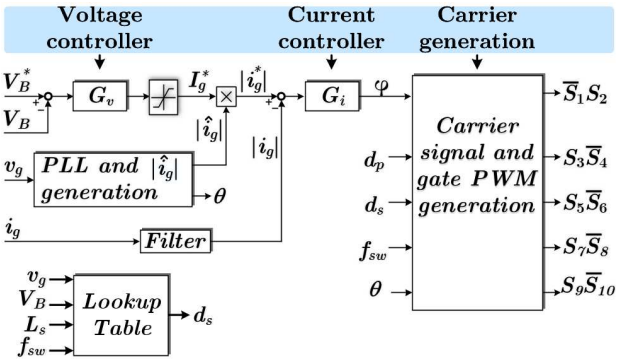

Fig. 5 Proposed high power quality control block diagram of the proposed converter.

not considered.

In this article, these odd order harmonics available in [1] are compensated by varying φ which is generated by the controller. As a result, high power quality is achieved including at light load.

IV. Experiment Results

To confirm the validity of the proposed method, the experiment results are given from a 3.7kW prototype of a single-phase OBC module, as shown in Fig. 6 at 1kW power, 120V grid input voltage, and output battery voltage from 175 to 425V. The presented experiments results are obtained by scaling down both ac input and dc output voltage by half based on the 3.7kW system-designed parameters and prototype specifications, provided in TABLE II and TABLE III, respectively. Fig. 7 (a), and Fig. 7 (b) show experimental results to verify grid current *THD* at a battery voltage of 300V, and different output power of 0.4kW and 1kW, respectively. Besides, the resulting grid current *THD* while using the conventional method [2] and the proposed method are compared at a battery voltage of 300V and an output power from 0.2kW to 1kW, as shown in Fig. 9 (a).

Fig. 8 (a) and Fig. 8 (b) show the worst-case *ZVS* turn-on waveforms at a battery voltage of 175V and 425V, respectively. The *ZVS* turn-on is achieved from 175 to 425V for all switches at a grid input voltage of 120V.

TABLE II
SYSTEM PARAMETERS OF THE PROPOSED ONBOARD CHARGER

Symbol	Description	Values
L_{g1}, L_{g2}	Grid inductors	30μH, SAMHWA ELECTRIC
L_s	Series inductor	40μH, SAMHWA ELECTRIC
S_1-S_{10}	Switches	NVBG020N120SC1
C_c	Clamping capacitor	1.6μF, [0.1μF MLCC] ×16
C_o	Output filter capacitor	10μF, [5μF film Capacitor] ×2

TABLE III
PROTOTYPE SPECIFICATIONS OF THE PROPOSED OBC AND TESTED VALUES

Symbol	Description	Nominal values	**Tested values**
P_o	Output power	3.7kW	**0.2 to 1kW**
V_g	Grid input voltage (RMS)	240V	**120V**
V_B	Battery output voltage	350 to 850V	**175 to 425V**
I_{g_peak}	Maximum grid current	16 A	**8 A**
I_{B_max}	Maximum battery current	14.4 A	**7.2 A**
f_{sw}	Switching frequency	150 kHz	**150 kHz**

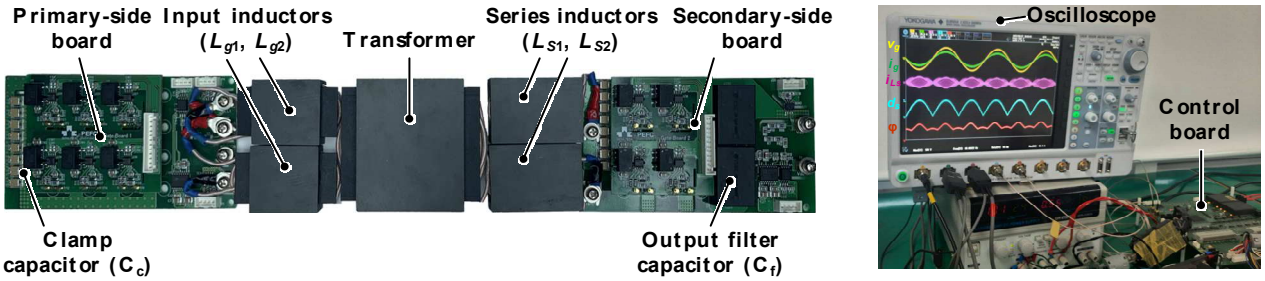

Fig. 6. The photograph of the 3.7kW OBC prototype built from a single-stage totem pole bidirectional ac to dc converter.

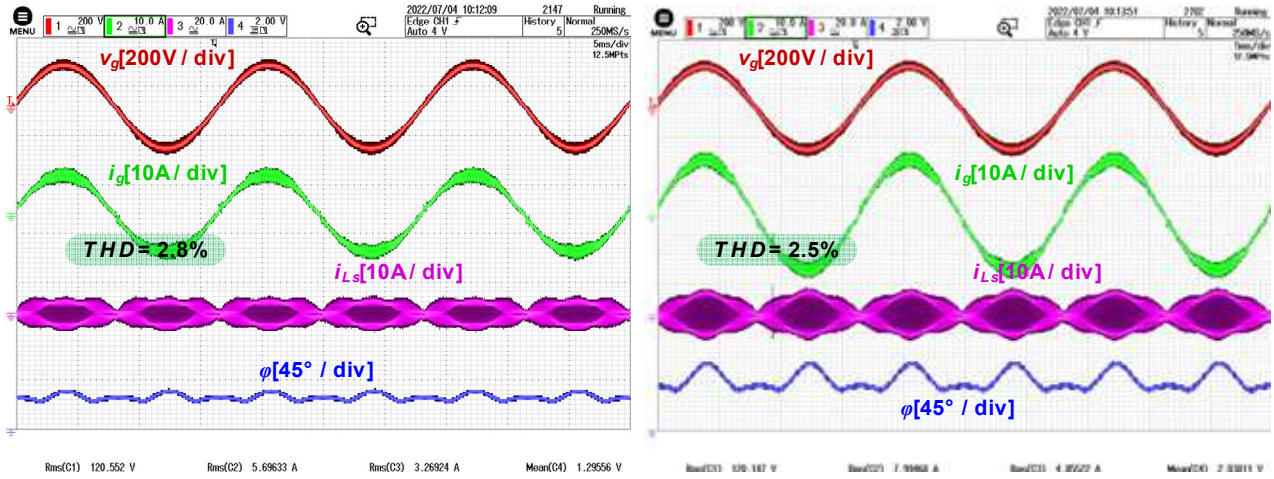

(a) (b)

Fig. 7: Experimental results showing the power quality by proposed real-time power regulation by using varying φ output by the controller at a grid voltage V_g=120V, battery voltage V_B = 300V, and different power; (a) P_o = 600W. (b) P_o = 1kW.

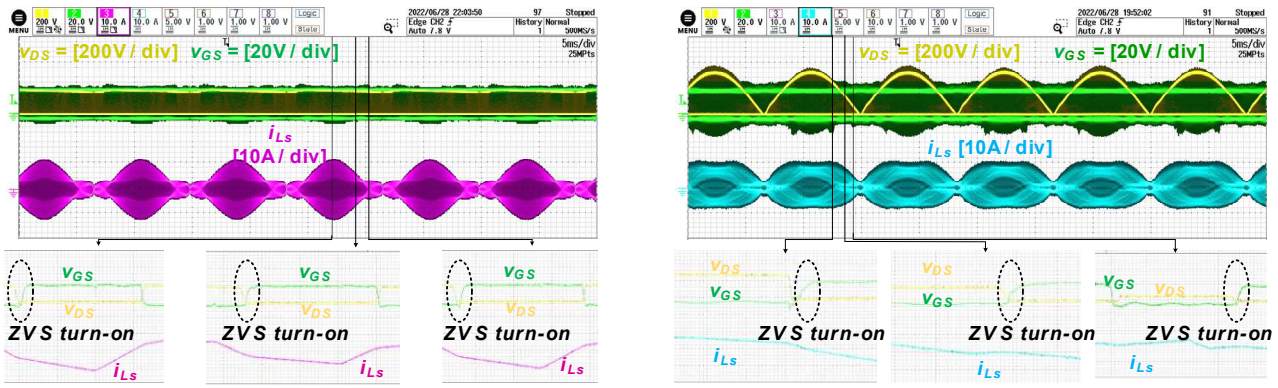

(a) (b)

Fig. 8 Worst case ZVS turn-on waveforms at V_g = 120V, for (a) Secondary switch S_8, at V_B=175V. (b) Primary switch S_4, at V_B=425V.

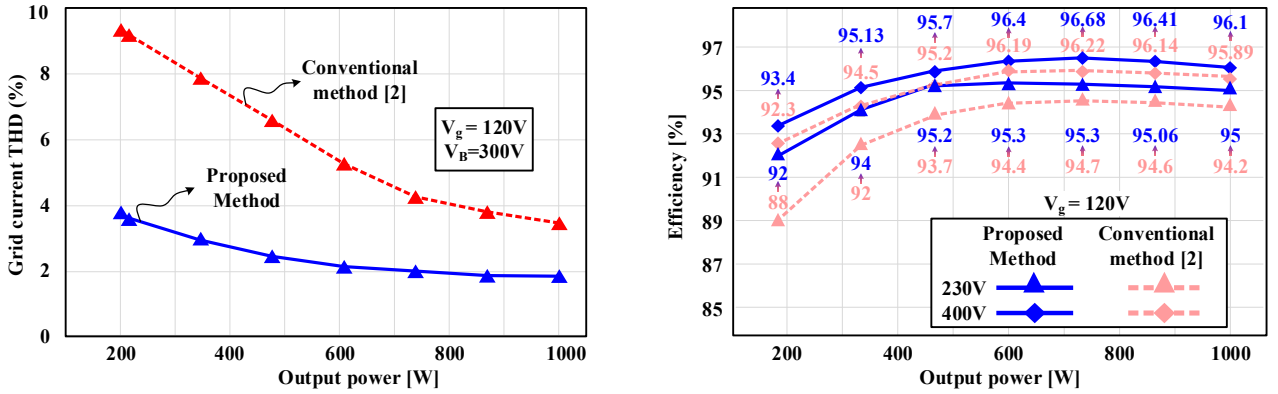

(a) (b)

Fig. 9. Comparison between the proposed method and the conventional method [2]. (a) Grid current THD. (b) Converter efficiency at two battery voltages of 230V and 400V.

That means that if the grid input voltage is scaled up to 240V, *ZVS* turn-on can be achieved from 350 to 850V battery with a full power transfer capability of 3.7kW.

The efficiency and power quality achieved by the proposed method and the conventional method [2] are compared under the same conditions. Fig. 9 (b) shows the efficiency comparison of the conventional method and the proposed method at battery voltages of 230V and 400V for output power from 0.2 to 1kW at a grid input voltage of 120V. As a result, the peak efficiency of the converter is increased by more than 0.4%, and light load efficiency is increased by more than 3% compared to [2].

V. Conclusion

High-efficiency and high-power quality modulation strategies are presented based on an optimal operation of single-stage control variables. To validate the theoretical claims, a 3.7kW prototype was built and tested at 1kW which is 25% of full power. With the proposed method, full *ZVS* turn-on is achieved for all switches over a wide voltage range from 175 to 425V battery voltage, circulating current is minimized, and high-power quality is achieved. Compared to the conventional method in [2] the efficiency of the converter is improved by 0.4% and 3% at 1kW power and light load, respectively. Grid-current *THD* of less than 4% is achieved including at light load, which satisfied the requirement by *IEEE*-1547 standard. Therefore, this method is good for application where high efficiency and high-power quality is required.

Acknowledgment

This paper was supported by the National Research Foundation of Korea, funded by the government (Ministry of Science and ICT) (No. 2020R1A2C2006301).

References

[1] H. Belkamel, H. Kim and S. Choi, "Interleaved Totem-Pole ZVS Converter Operating in CCM for Single-Stage Bidirectional AC–DC Conversion with High-Frequency Isolation," in *IEEE TPE*, vol. 36, no. 3, pp. 3486-3495, March 2021, doi: 10.1109/TPEL.2020.3016684.

[2] H. Kim, J. Park, S. Kim, R. M. Hakim, H. Belkamel and S. Choi, "A Single-Stage Electrolytic Capacitor-Less EV Charger With Single- and Three-Phase Compatibility," *in IEEE TPE, vol.37, no. 6, pp.*

6780-6791, June 2022, doi: 10.1109/TPEL.2021.3127010.

[3] D. Das, N. Weise, K. Basu, R. Baranwal and N. Mohan, “A Bidirectional Soft-Switched DAB-Based Single-Stage Three-Phase AC–DC Converter for V2G Application,” *in IEEE TTE,* vol. 5, no. 1,pp.186-199, March 2019, doi: 10.1109/TTE.2018.288645.

[4] F. Jauch and J. Biela, "Combined Phase-Shift and Frequency Modulation of a Dual-Active-Bridge AC–DC Converter With PFC," *in IEEE TPE,* vol. 31, no. 12, pp. 8387-8397, Dec. 2016, doi: 10.1109/TPEL.2016.2515850.

[5] J. Lu et al., "A Modular-Designed Three-Phase High-Efficiency High-Power-Density EV Battery Charger Using Dual/Triple-Phase-Shift Control,” *in IEEE, TPE,* vol. 33, no. 9, pp. 8091-8100, Sept. 2018, doi: 10.1109/TPEL.2017.2769661.

[6] Y. Cho, W. Cha, J. Kwon and B. Kwon, "High-Efficiency Bidirectional DAB Inverter Using a Novel Hybrid Modulation for Stand-Alone Power Generating System with Low Input Voltage,” in *IEEE TPE,* vol. 31, no. 6, pp. 4138-4147, June 2016, doi: 10.1109/TPEL.2015.2476336.

[7] O. Kwon, K.-S. Kim and B.-H. Kwon, "Highly Efficient Single-Stage DAB Microinverter Using a Novel Modulation Strategy to Minimize Reactive Power,” *in IEEE Journal of Emerging and Selected Topics in Power Electronics*, vol. 10, no.1, pp.544-552, Feb.2022, doi: 10.1109/JESTPE.2021.3090097.

[8] Z. Guo and X. Han,” Control Strategy of AC-DC Converter Based on Dual Active Bridge with Minimum Current Stress and Soft Switching,” *in IEEE, TPE*, vol. 37, no. 9, pp. 10178-10189, Sept. 2022, doi: 10.1109/TPEL.2022.3153626.

[9] Million Gerado Geda, Tat-Thang LE, Huu-Phuc Kieu, Sunju Kim, Sewan Choi." A New ZVS Modulation Strategy for Single-Stage Electrolytic Capacitor-less On-board Charger "*Power Electronics Conference*,(2022):297-299.